 doi:10.20944/preprints202207.0248.v1

Article

Urban Sprawl and Its Influence on Land Surface Temperature: A Case Study of Bagdad City from 1985 to 2021

Azad Rasul

[1] Soran University, Department of Geography, Soran, Erbil, Iraq
*Corresponding author: azad.rasul@soran.edu.iq

Abstract: Land Use Land Cover (LULC) change and urban growth have a significant influence on local climate of cities. From 1985 to 2021 the population of Baghdad increased by 103%. Therefore, the risen question is how this expansion influences the temperature of the city. The study aims to identify urban growth of Baghdad, investigate its influence on variation of Land Surface Temperature (LST) and identify the main factors that control the surface temperature of the city. Three Landsat images from 1985 to 2021, in addition to sixteen potential factors, were used in the study. Our findings suggest that during the study period, vegetated areas declined by 39% while built-up class increased by 139%. Bare soil recorded the highest surface temperature. The study found that surface temperature has a strong inverse relationship with vegetation (Normalized Difference Vegetation Index (NDVI): $r = -0.62$, $p < 0.001$) and moisture (Normalized Difference Moisture Index (NDMI): $r = -0.65$, $p < 0.001$). Therefore, increasing vegetation and water body lead to decrease temperature of the city. Our findings help policymakers to deal with climatic issues rising from urban growth of the city.

Keywords: Landsat; urban growth; Land Use Land Cover (LULC); remote sensing; urbanisation; NDVI

1. Introduction

Recently, there has been a great deal of interest in urban sprawl and its relation to urban climate. However, a remaining common question in the field is how urban expansion influences the temperature of the city in different climatic regions and environmental backgrounds. Iraq faced a fast population expansion with an increasing rate of 170%. At the start of this study period (1985), its population was 15,555,800 people while currently (2022) it is estimated to be 42 million inhabitants. In addition, it is forecasted to reach more than 70 million by 2050 ("Iraq Population (2022) - Worldometer," 2022). Baghdad as capital and dense city of Iraq gained a high rate of this growth. During year1985 the population of Baghdad the capital of Iraq was about three and a half million, but in 2021 the population of the city estimated by more than seven million, meaning it is increased by 103%.

The land surface is a combination of vegetation, water surfaces, impervious materials and exposed soils. As a result of the complexity of the surface, Land Surface Temperature (LST) varies spatiotemporally (Rasul et al., 2017). Water body, soil moisture and vegetation through evaporation, evapotranspiration and latent heat flux decrease surface temperature. Therefore, there is a relationship between LST and LULC (Azad Rasul et al., 2016). Therefore, radical changes could occur in a newly urbanised area. Usually, the urban expansion leads to a raised surface temperature in humid environments while it may lead to a decrease in surface temperature of urbanised areas in arid environments during daytime compared to dry surroundings (Cai and Du, 2009; Rasul et al., 2015; Shigeta et al., 2009).

Besides metrological data, surface temperature is measured from different remote sensing platforms such as satellite, aircraft and unmanned aerial vehicle (UAV). Surface temperature obtained from satellite sensors is capable to be used in the study of climate of urban areas and spatial variation of LST (Watson, 2012). Because Landsat series have a

Preprints (www.preprints.org) | NOT PEER-REVIEWED | Posted: 18 July 2022 doi:10.20944/preprints202207.0248.v1

long record, are freely available and have a suitable resolution for urban studies, among satellite sensors, it is widely used to analyse the spatiotemporal variation of LST and relationship between LST and land use change (Rasul et al., 2015; Traore et al., 2021; Xian et al., 2022).

However, the influence of urban sprawl on temperature of the cities in hot desert climates *(BWh)* such as Baghdad has rarely been investigated. Therefore, one of the important question rasing is how replacing vegetated and bare soil areas with built-up class during the last four decades influenced the climate of the city, especially, the temperature in the global warming era. Therefore, the goal of this study was to 1. identify LULC change of Baghdad from 1985 to 2021 2. assess spatiotemporal variation of LST of Baghdad 3. identify the main factors that control surface temperature of the study area. To achieve these objectives, the study analysed Landsat images from 1985 to 2021 and sixteen potential factors such as Dry Built-up index (DBI), Dry Bare-soil Index (DBSI), Enhanced Vegetation Index (EVI), Normalized Difference Vegetation Index (NDVI), Normalized Difference Moisture Index (NDMI), Normalized Difference Latent Heat Index (NDLI), impervious surface and population number. Results of the study assist policymakers and municipality administrations to mitigate the temperature of the city, especially during the summertime and hit waves by providing significant information regards LULC of Baghdad and its influence on the surface temperature of the city.

2. Materials and methods

2.1. Study area

Our case study is Baghdad city and the square corridor around it. It is laid between 33 10 38 to 33 30 10 N latitude and 44 09 26 to 44 32 07 E longitude. Baghdad is the capital, the densest and most populated city in Iraq. It is situated in the centre of Iraq on both sides of the Tigris River. It is elevation is 23m in the south and 48m MSL in the north (Ali and Ramahi, 2020). The population of the city is about 7,500,000 people, covering an area of about 205 km^2. The Tigris splits the city into two sections: Karkh in the west and Rusafa in the east (Ali and Ramahi, 2020). The climate of the city is described as cold and humid during winter and hot and dry during the summer (Abdul-Hammed and Mahdi, 2022).

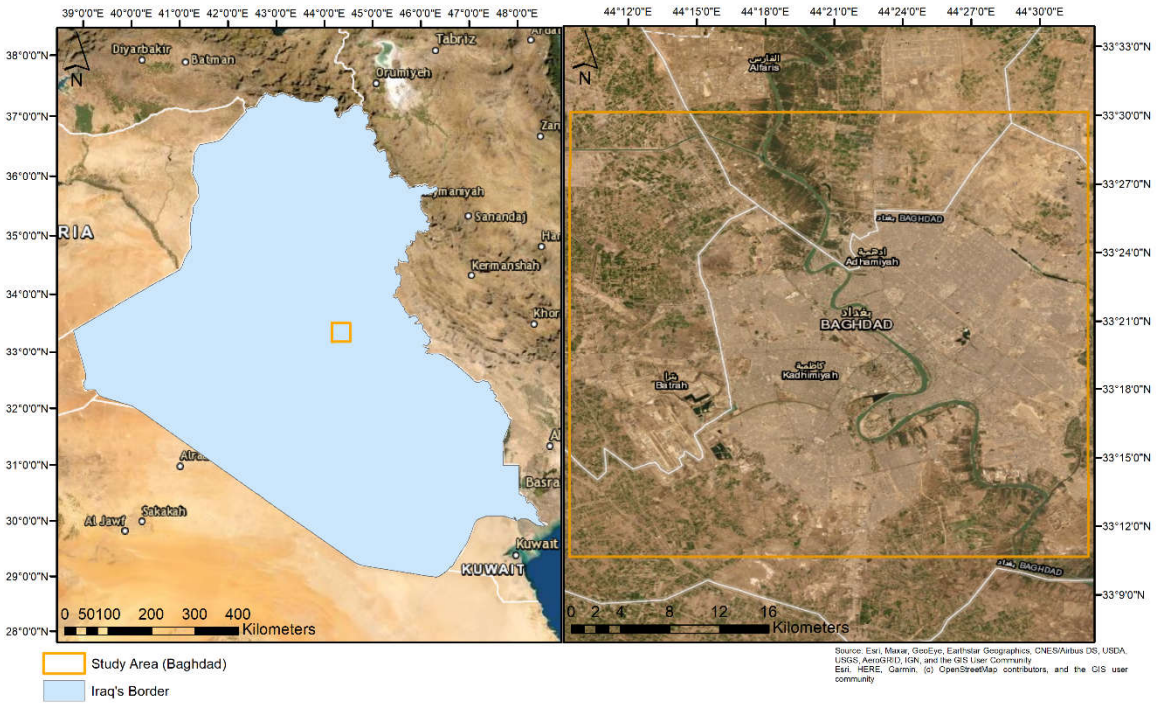

Figure 1. location of the study area.

Preprints (www.preprints.org) | NOT PEER-REVIEWED | Posted: 18 July 2022 doi:10.20944/preprints202207.0248.v1

2.2. Data

In the study, we used three Landsat images, the first image is Landsat 5 was acquired on 29 July 1985, the second is Landsat 7 was acquired on 14 July 2000 and the third is Landsat 8 and acquired on 23 July 2021. All used images were acquired during the dry season and in the same month (July). These images were processed and converted to LST and LULC indices using Google Earth Engine (GEE), cloud based remote sensing platform.

2.3. Methods

2.3.1. Estimation of Land Surface Temperature

LST of used Landsat 5, 7 and 8 series estimated through GEE using the code of (Ermida et al., 2020). All used data resampled to 30m. In the process of converting raw data to LST Statistical Mono-Window (SMW) algorithm (Equation 1) has been used. The algorithm performed atmospheric correction of Landsat thermal band series using atmospheric data provided in GEE, the re-analyses of the National Center for Environmental Prediction (NCEP) and National Center for Atmospheric Research (NCAR) (Kalnay et al., 1996). Although, surface emissivity correction was performed using Landsat TIR bare ground emissivity. FVC values for the Landsat image are extracted from NDVI values using Equation 2 and emissivity of each pixel of band is extracted using Equation 3.

$$LST = A_i \frac{Tb}{\varepsilon} + B_i \frac{1}{\varepsilon} + C_i \quad (1)$$

where Tb is the TOA brightness temperature in the thermal channel, and ε is the surface emissivity for the used channel. The algorithm coefficients A_i, B_i; and C_i are determined from linear regressions of radiative transfer simulations executed for 10 classes of Total Column Water Vapor (TCWV).

$$FVC = \left(\frac{NDVI - NDVI_{bare}}{NDVI_{veg} - NDVI_{bare}}\right)^2 \quad (2)$$

where FVC is fraction vegetation cover, $NDVI_{bare}$ and $NDVI_{veg}$ are the NDVI values of fully bare and completely vegetated pixels, respectively.

$$\varepsilon = 0.004 * FVC + 0.986 \quad (3)$$

where, 0.004 represents the average emissivity value of bare land, 0.986 correspondents to the values of average emissivity of the vegetated land.

Estimated LST images downloaded to a local computer. Then, Normalized Ratio Scale (NRS) statistical method (Equation 4) is used in R Programming to normalize variables of LST acquired during different periods and climatic situations and make them comparable to each other.

$$LST_{NRS} = \frac{LST}{\sqrt{\sum (LST)^2}} \quad (4)$$

where LST is the value of each pixel in LST image. To return the values similar to the original LST values, LST_{NRS} is multiplied by the results of Equation (5):

$$N = \frac{\overline{x_1}}{\overline{x_2}} \quad (5)$$

where $\overline{x_1}$ is the mean LST of original image and $\overline{x_2}$ is the mean of the normalized LST image (from Equation (4)).

2.3.2. Image classification

Since previous studies proved that, the performance of Random Forest (RF) is higher than other classifiers in GEE (Goldblatt et al., 2016; Rasul et al., 2021), the RF procedure was selected in this study. GEE is used in this study for the image classification. The main steps

 doi:10.20944/preprints202207.0248.v1

are selecting images of Landsat within three periods, selecting samples of testing and validation points, generating classified maps, and evaluating accuracy of classified maps.

For all used Landsat images, Random Forest method is used to classify Landsat images to LULC. Because Landsat image has only 30m resolution, we classified images into four main classes in the area namely, water body, vegetation (grass, tree and agriculture), built-up (building, road, pavement) and bare soil (rock, bare soil, crop areas dry during summer season).

In image classification, 400 samples were selected for each image; 100 samples of each class. Samples were chosen based on the high resolution satellite image available as basemap in GEE, prior knowledge of researcher, and true and false band compositions of Landsat images. Samples are divided into two categories; 70% of samples are used for training points and 30% of samples are used as testing points for validation. In the algorithm, after testing an RF classifier for best performance, 40 decision trees were used. In addition, some techniques are used to improve the accuracy of the method, namely, adding LULC indices (NDVI, NDWI, DBI, DBSI) to original Landsat bands and normalization of values to be between 0 to 1. Areas of each class and accuracy values are extracted, and then, classified images are exported from GEE to Google Drive and then to a local computer to perform analysis and visualization.

To assess the accuracy of classified images, we measured evaluation classifiers as overall accuracy (OA), Kappa coefficient, producer accuracy, and user accuracy. Overall accuracy verifies the overall efficiency of the method that is calculated by dividing the total number of correctly considered samples by the total number of the testing samples. Whereas, the Kappa coefficient exhibits the degree of agreement between the validation samples and the predicted values (Goldblatt et al., 2017). To perform accuracy assessment, Kappa and overall accuracy were derived by utilizing error Matrix of classified Landsat images.

2.3.3. Land Use Land Cover variables

The research used a list of LULC products available in GEE, namely, Tree Canopy Cover, population number, built Up Multitemporal, Degree of Urbanization, nighttime light, elevation, and impervious change year. In addition, a list of LULC indices was generated in the GEE, using equations in Table (1), namely, Normalized Difference Water Index (NDWI), NDLI, NDVI, EVI, DBSI, DBI, NDMI, Normalized Soil Moisture Index (NSMI). In addition, slope of the study area is calculated using the 4-connected neighbours of each pixel using “ee.Terrain.slope” function in GEE. Then, raster images of these variables were downloaded to a local computer through Google Drive for performing analysis.

Preprints (www.preprints.org) | NOT PEER-REVIEWED | Posted: 18 July 2022 doi:10.20944/preprints202207.0248.v1

Table 1. mathematical formulas of calculated indices in the study.

Index	Equation	Reference
Enhanced Vegetation Index	$\boldsymbol{EVI} = 2.5 \times \frac{(NIR - RED)}{(NIR + 6 \times RED - 7.5 \times BLUE + 1)}$	(Jiang et al., 2008)
Normalized Different Vegetation Index	$\boldsymbol{NDVI} = \frac{(NIR - RED)}{(NIR + \mathrm{RED})}$	(Rouse et al., 1973)
Normalized Different Water Index	$\boldsymbol{NDWI} = \frac{(GREEN - NIR)}{(GREEN + NIR)}$	(McFeeters, 1996)
Normalized Difference Latent Heat Index	$\boldsymbol{NDLI} = \frac{(GREEN - RED)}{(GREEN + RED + MIR)}$	(Liou et al., 2018)
Dry Built-up Index	$\boldsymbol{DBI} = \frac{(BLUE - TIR1)}{(BLUE + TIR1)} - NDVI + 2$	(Rasul et al., 2018)
Dry Bare-soil Index	$\boldsymbol{DBSI} = \frac{(SWIR1 - GREEN)}{(SWIR1 + GREEN)} - NDVI$	(Rasul et al., 2018)
Normalized Difference Moisture Index	$\boldsymbol{NDMI} = \frac{(NIR - SWIR1)}{(NIR + SWIR1)}$	(Wilson and Sader, 2002)
Normalized Soil Moisture Index	$\boldsymbol{NSMI} = \frac{(SWIR1 - SWIR2)}{(SWIR1 + SWIR2)}$	(Haubrock et al., 2008)

2.3.4. Statistical analysis

Values of 300 random samples were extracted for LULC variables and LST. To better represent the different indices to LULC categories and study the association of these classes with LST, pixels with low values were masked out. For NDVI and EVI vegetation indices, pixels with 0.2 or fewer values and water body NDWI less than -0.2 are ignored (sentinel-hub, 2019, 2018).

Statistical calculations were performed in R programming. To assess the relationship between LST and explanatory LULC variables, we used univariate regression of Pearson's product-moment (Equation 4). The significance of the relationship was tested with student's t-test (Equation 5).

$$R = \frac{\sum(x - \bar{x})(y - \bar{y})}{\sqrt{\sum(x - \bar{x})^2 \sum(y - \bar{y})^2}} \quad (6)$$

where x is value of LULC indices, $\bar{x}$ is mean of values of LULC indices, and y is LST value, $\bar{y}$ is mean of the values of the y-variable. A result close to +1 indicates a strong positive correlation while a result close to -1 represents a strong negative correlation. A value of zero means no correlation exists between variables.

$$t = \frac{r\sqrt{n-2}}{1-r^2} \quad (7)$$

where r is the sample correlation coefficient and n is the number of cases.

3. Results

The objective of the study is to identify urban sprawl of Baghdad, investigate variation of LST and identify the main factors that influence the surface temperature of the city. To achieve these objectives, in this section, we display our findings on LST and LULC classification from 1985 to 2021. In addition to spatial variation of 16 LULC variables that are considered in this study. Then results of association between these factors and LST will be illustrated.

3.1. Spatiotemporal distribution of Land Surface Temperature in Baghdad

Figure 2 (a:c) shows that lower LST (blue colour from 300 to 320 k) is associated with water (Tiger River), vegetated area in the north and the south of the city mainly around

Preprints (www.preprints.org) | NOT PEER-REVIEWED | Posted: 18 July 2022 doi:10.20944/preprints202207.0248.v1

the river, and built-up area in the centre of the area. The higher temperature area (325-350 k) is mainly collocated with bare soil and winter croplands that dry during summer. The hottest area is located in the northeast of the city. Figure 2 (b and e) shows that during the year 2000 with converting bare soil to built-up area, lower LST areas increased. However, during the satellite time passing of 2021, generally, LST is higher compared to 1985 and 2000, especially in the north part of the city where LST reached 350 k.

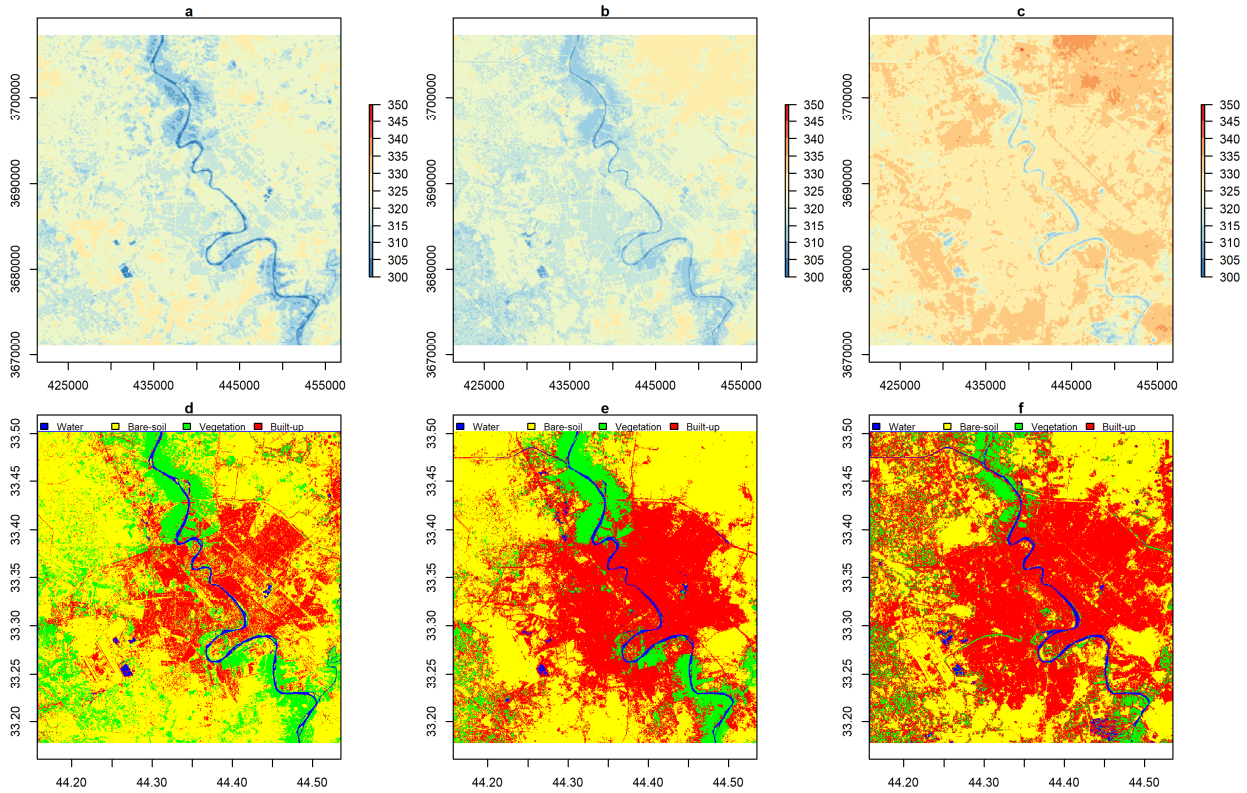

Figure 2. spatiotemporal variation of LST (in K) and LULC classification from 1985 to 2021. a: LST of 1985, b: LST of 2000, c: LST of 2021, d: LULC of 1985, e: LULC of 2000 and f: LULC of 2021. Blue: water, yellow: bare soil, green: vegetation and red: built-up class.

3.2. Land Use Land Cover variation of Baghdad from 1985 to 2021

In general, the accuracy of our classification is high in all three classified images. Techniques used to improve the accuracy of the method led to more increase in the accuracy. Namely, adding LULC indices to original Landsat bands and increasing number of trees from 10 to 40 in Random Forest increased both Kappe and total accuracy, however, normalization of values to be between 0 to 1, does not lead to rise in the accuracy. The total accuracy and Kappa of all three classified images were 0.97 and higher (Table 2). The highest total accuracy and kappa (0.99) were achieved in classified Landsat 8 image of 2021.

Table 2. accuracy assessment of LULC classification based on Random Forest algorithm.

Year	Total accuracy	Kappa
1985	0.98	0.98
2000	0.98	0.97
2021	0.99	0.99

Preprints (www.preprints.org) | NOT PEER-REVIEWED | Posted: 18 July 2022 doi:10.20944/preprints202207.0248.v1

Table 3. area of classes and changes from 1985 to 2021 using Landsat images.

Class	1985(km^2)	1985%	2000(km^2)	2000%	2021(km^2)	2021%	2021-1985(km^2)
Water	19.8	1.6	18.3	1.4	19.5	1.5	-0.3
Bare soil	758.7	60.1	601.8	47.5	455.5	36.1	-303.1
Vegetation	207.7	16.5	145.1	11.5	126.1	10.0	-81.6
Built-up	276.3	21.9	500.7	39.5	661.2	52.4	385.0
Total	1262.4	100.0	1265.9	100.0	1262.4	100.0	

In the first year of the study time (1985), the main class of study area was bare soil (758.7 km^2, 60.1%), built-up class came in the second order (21.9%, Figure 3). Vegetated class came in the third order and covered only 16.5% (Table 3, Figure 2 d:f). After fifteen years, in 2000 bare soil stay in the first main class, however, it declined to 47.5% (601.8 km^2). Built-up class stayed in the second order between classes, in contrast, it increased dramatically from 276 to 500 km^2 (21.9 to 39.5%). Meanwhile, vegetation class has fallen from 16.5 to only 11.5%. In classified Landsat 8 during 2021 of the same month (July), built-up class came in the first order (52.4%, 661 km^2). In contrast, bare soil has fallen to only 36.1% of the area and vegetation decreased more to only 10%. Regarding water class, it changed slightly during the study period. Comparing area of each class between 1985 and 2021 displays that built-up area increased dramatically by 139.3% (385km^2), in contrast, bare soil and vegetation lost 303 (41.3%) and 81.6 km^2 (39.3%), respectively (Figure 4).

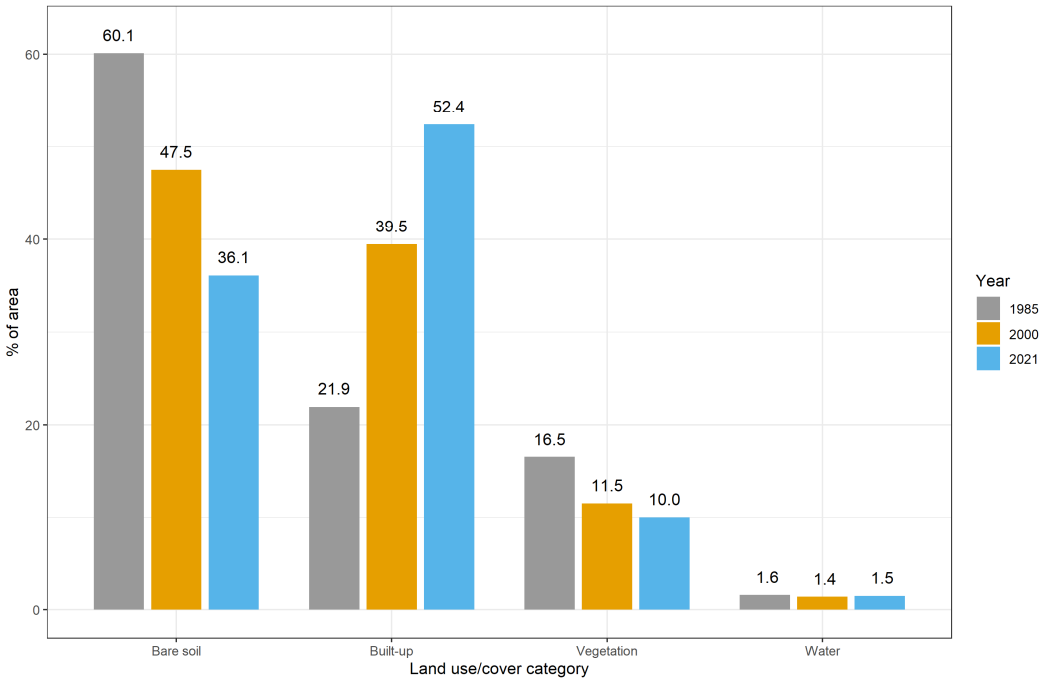

Figure 3. Percentage area of LULC classes of Baghdad city from 1985 to 2021.

Preprints (www.preprints.org) | NOT PEER-REVIEWED | Posted: 18 July 2022 doi:10.20944/preprints202207.0248.v1

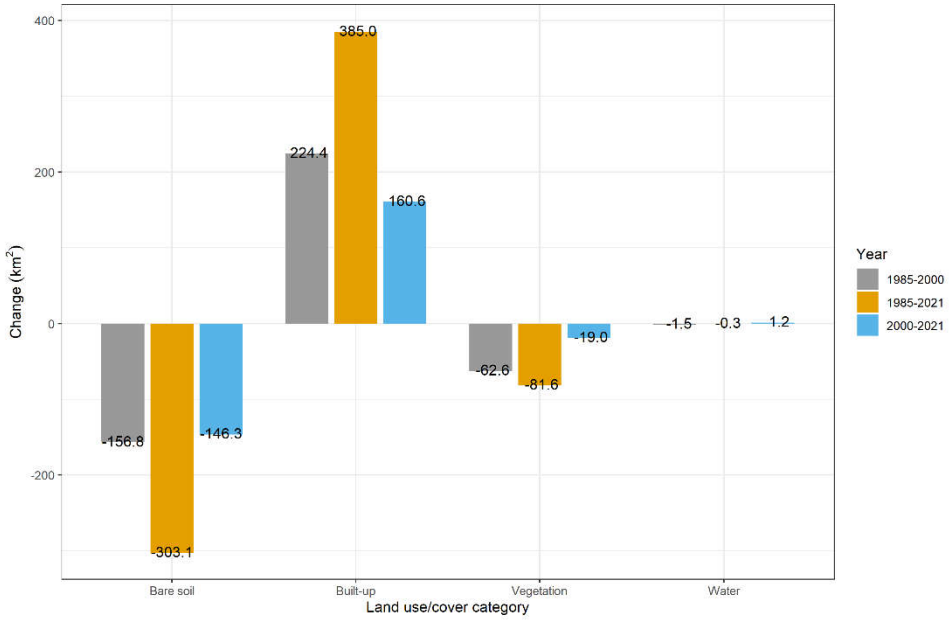

Figure 4. LULC change in Baghdad city during 1985–2021.

3.3. The difference of LST between LULC classes

During all analysed years (1985, 2000, 2021) bare soil class recorded the highest LST (322.5, 322.7, 331.3 k) followed by built-up class (320.9, 320.1, 327.9 k). In contrast, water bodies and vegetation areas recorded lower temperatures (Figure 5). In general surface temperature during 2021 of all classes was higher than surface temperature of these classes during 1985 and 2000.

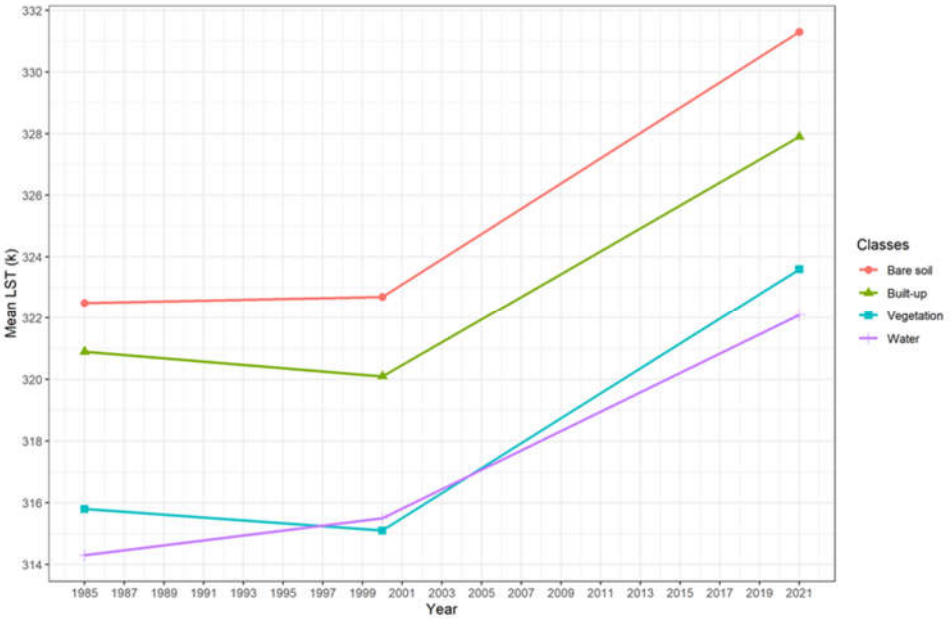

Figure 5. The differences of mean LST over different land cover types in 1985, 2000 and 2021 in Baghdad.

3.4. Spatial distribution of land cover variables

Areas with higher than 0.8 DBI are considered built-up areas that occupied the most of the study area during 2021. While dark brown with more than 1 DBI considered of highly built-up area which occupied some polygons on the right side of the Tiger River (Figure 6:a). Bare soil areas are located in the surrounding the built-up area. It is coloured

 doi:10.20944/preprints202207.0248.v1

brown with 0.2 and higher BDSI, especially in the right top corner of the study area (Figure 6:b). NDVI and EVI (Figure 6:c,f) display that a densely vegetated area with more than 0.4 NDVI is mainly located in the north part of the city around Tiger River and the second highest vegetation area is located on the bottom right side of the study are. While a separated plot of vegetation is located in the western part of Baghdad. These areas with high vegetation indices are associated with low surface temperature with dark blue colour in Image 6:i.

Very low NDLI is associated with bare soil area in the right top of the area (brown colour) while more than 0.1 NDLI is associated with water and vegetated places around the Tiger River (Figure 6:d). NDWI with 0.2 and higher displays Tiger River from top to the bottom of the area. In addition, some water plots are located in the west part of the area (Figure 6:g). This high NDWI colocated with relatively low surface temperature (Figure 6:i). Low moisture is located in the built-up and bare soil area in the city while high moisture is mainly located in the north and bottom right side of the city within the vegetated area in addition to some separate plots on the west side of the area (Figure 6:e,h). These high moisture areas lead to decrease surface temperature (Figure 6:i).

Figure 7:a shows elevation of the study area. Low altitude arias (20m) are located in the south part and north west of the study area. Impervious surface with value 30 and higher (brown colour) display the built-up area while low impervious value in green colour surrounding the city. Dense impervious area associated with middle surface temperature with light blue colour (Figure 7:h). The highest night light was plotted in the north part of the study area (Figure 7:c). Figure 4:d displays that only a small portion in the north part of the study area has high trees and around 5 value tree canopy cover. Highest urbanised (3 value) pixels were coloured with dark red and covered most of the study area (Figure 7:e). Rural areas are coloured green in the north, south and west part. Densely populated area (60 value and higher) of the city with brown colour located in the east and the surrounding the Tiger River. Low populated areas surrounded the city (Figure 7:f). Figure 7:g shows the slope of the study area and releases that spot with a high slope (<30m) located in the middle of the study area.

Preprints (www.preprints.org) | NOT PEER-REVIEWED | Posted: 18 July 2022 doi:10.20944/preprints202207.0248.v1

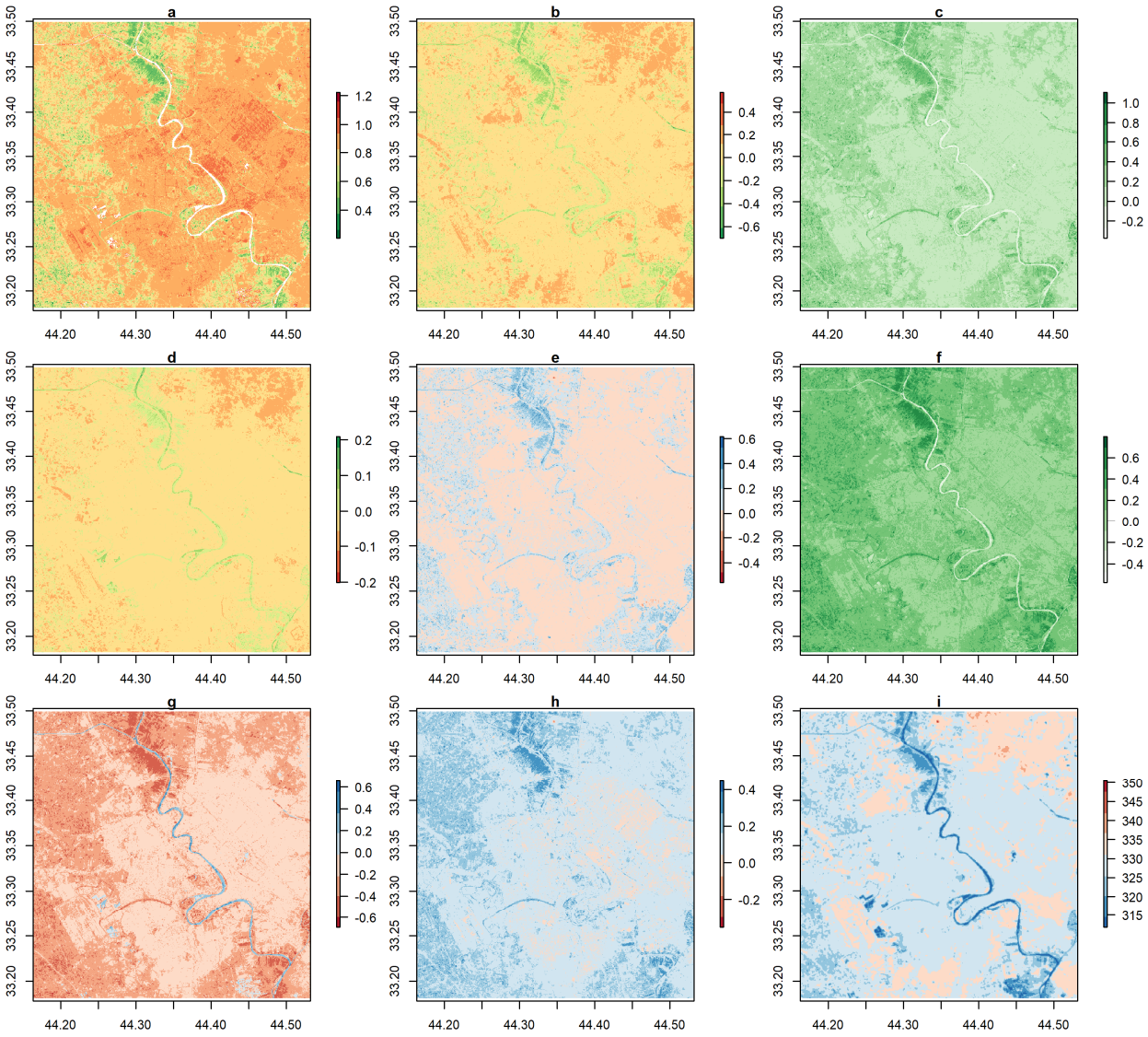

Figure 6. spatial variation of land cover variables and LST, a: DBI, b: DBSI, c: EVI, d: NDLI, e: NDMI, f: NDVI, g: NDWI, h: NSMI, i: LST.

Preprints (www.preprints.org) | NOT PEER-REVIEWED | Posted: 18 July 2022 doi:10.20944/preprints202207.0248.v1

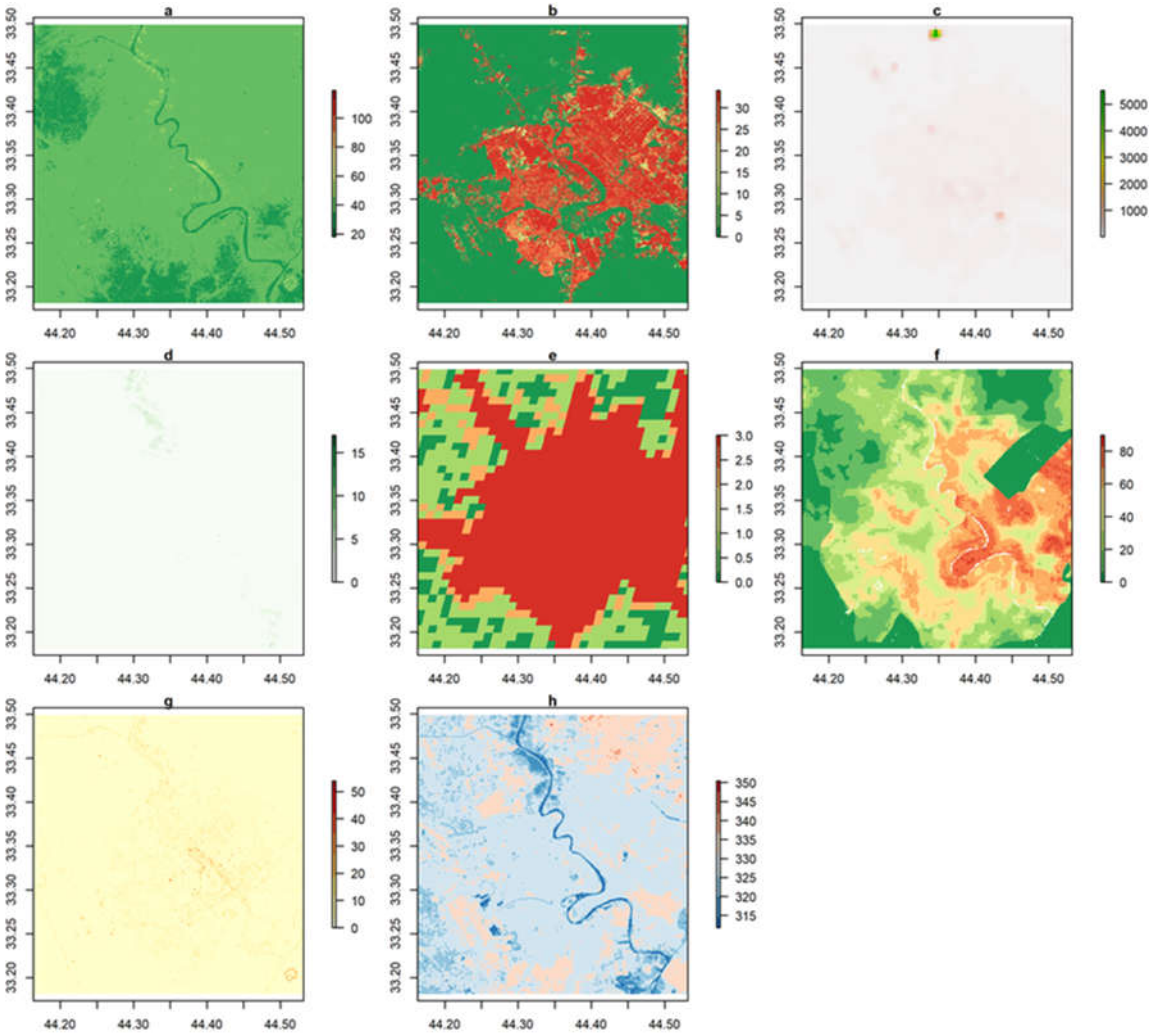

Figure 7. spatial variation of land cover variables and LST, a: dem, b: impervious, c: nighttime light, d: TCC, e: urban, f: population number, g: slope, h: LST.

3.5. Statistical analysis of relationship between potential variables and LST

A strong significant inverse association was found between LST and NDMI (r = -0.65), NDVI (r = -0.62), EVI (r = -0.58), NDLI (r = -0.68), NDWI (r = -0.6) and TCC (r = -0.5). In contrast, a strong significant positive correlation was found between LST and DBSI (r = 0.7) and DBI (r = 0.54) (Figures 8 & 9). A medium positive correlation was found between LST and degree of urbanisation (r = 0.32), however, a medium negative correlation was found with NSMI (r = -0.49).

In contrast, a small negative correlation was found between LST and slope (r = -0.15). No association or no statistically significant association was found between LST and population number, built-up multitemporal, impervious change year, nighttime light and dem (Figure 9).

Preprints (www.preprints.org) | NOT PEER-REVIEWED | Posted: 18 July 2022 doi:10.20944/preprints202207.0248.v1

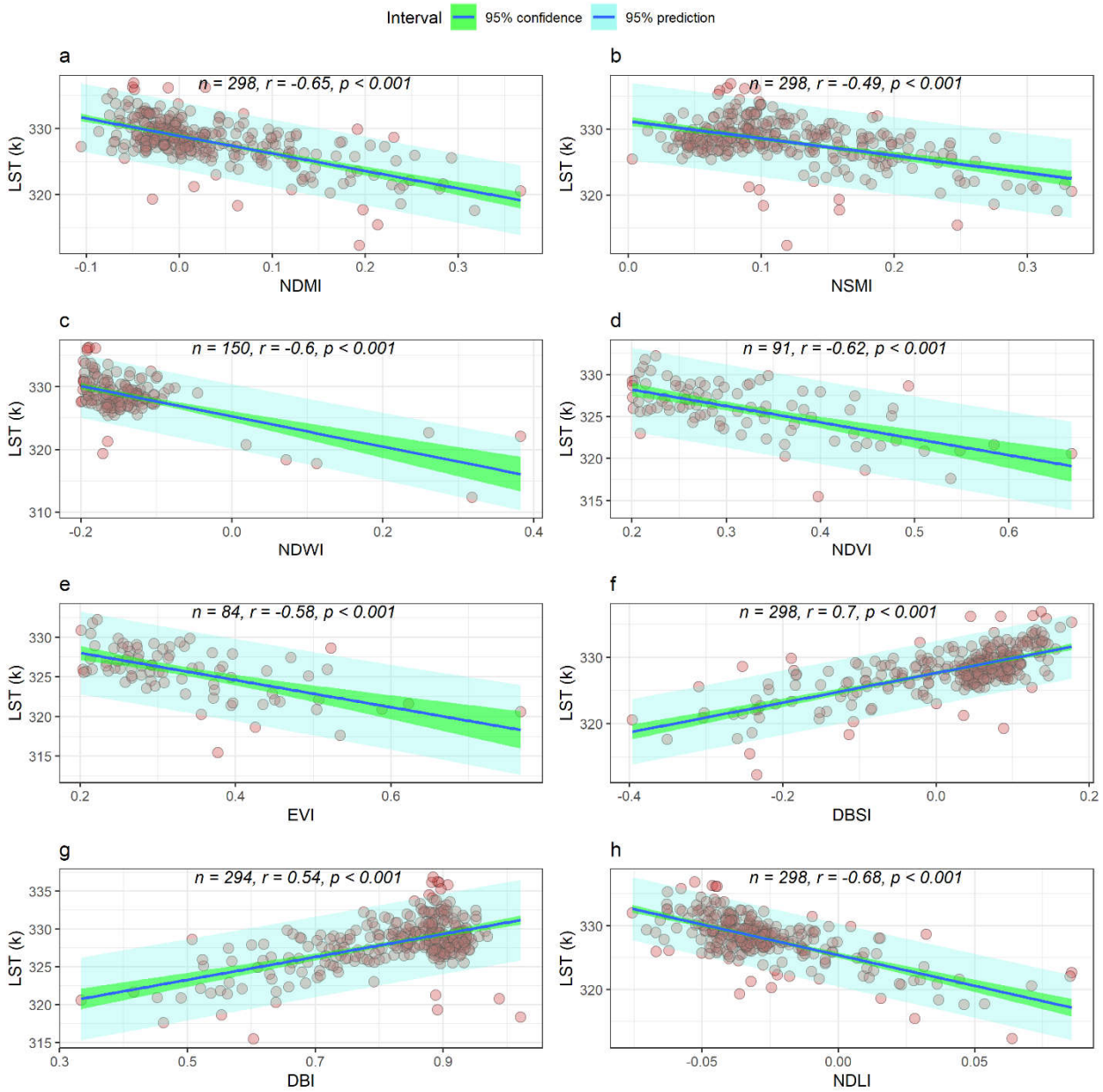

Figure 8. the relationship between potential variables and LST, a: NDMI, b: NSMI, c: NDWI, d: NDVI, e: EVI, f: DBSI, g: DBI, h: NDLI.

Preprints (www.preprints.org) | NOT PEER-REVIEWED | Posted: 18 July 2022 doi:10.20944/preprints202207.0248.v1

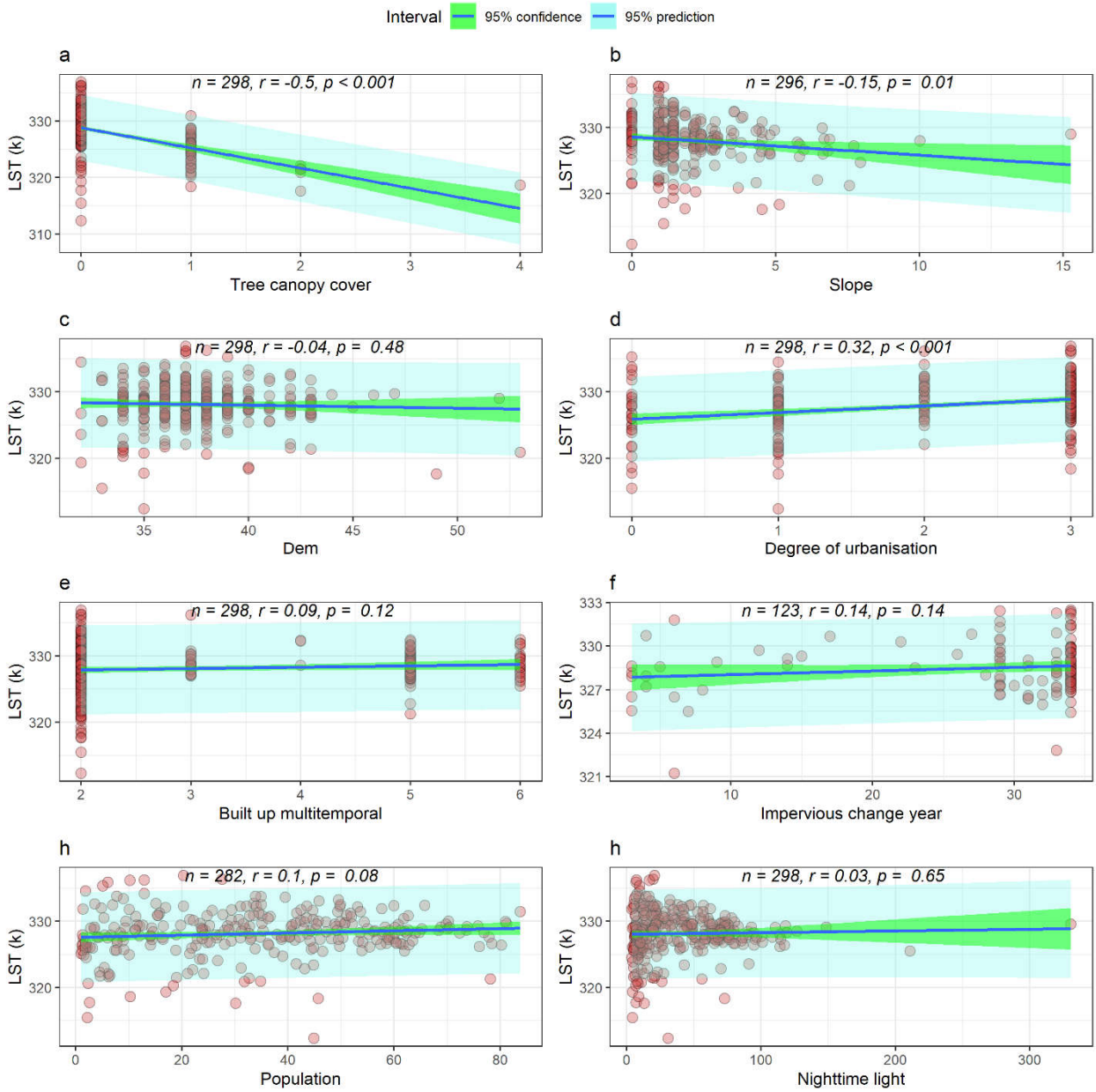

Figure 9. the relationship between potential variables and LST, a: TCC, b: slope, c: dem, d: degree of urbanisation, e: built-up multitemporal, f: impervious change year, g: population, h: nighttime light.

4. Discussion

The study find that hottest part is located in the north east of the city covered by bare soil. And achieved accuracy of our LULC classification was 0.98. In addition, during the study period, a significant change occurred in the main classes. From 1985 to 2021 built-up area increased by 139.3%, in contrast, vegetation area declined by 39.3%. Regarding variation of LST of land use class, bare soil recorded the highest surface temperature followed by built-up area. While vegetation and water body experienced lower surface temperatures. These areas of lower temperature were located in Tiver River and areas surrounding it from north west to south east of the study area.

The result of statistical analysis between surface temperature and potential factors revealed that the main factors that lead to decrease surface temperature are moisture (NDMI), vegetation area (NDVI, EVI and TCC) and latent heat (NDLI). While a positive strong correlation was found between LST and bare soil (DBSI) and built-up (DBI) indices.

 doi:10.20944/preprints202207.0248.v1

In other studies areas where non-urban land is dominated by vegetation (e.x. Atlanta), urban areas (mixed with imperviousness and vegetation) has larger LST (Xian et al., 2022). However, it is not right in all the parts of the world, that urbanized areas record the highest temperature compared to other land use classes. Therefore, in Bagdad, during the morning, which is the time pass of the Landsat satellite, bare soil experiences higher surface temperature than in urban areas. This result is consistent with the observations in arid land (Frey et al., 2005; Li et al., 2011; Rasul et al., 2015), but in contrast with (Amiri et al., 2009; Carlson and Arthur, 2000; Owen et al., 1998). This situation may be different during the nighttime when bare soil reflects its heat quickly and urbanized area could record higher temperature. In this case, the city experience an urban cold island during and daytime and an urban heat island during the nighttime.

Using improved techniques in our study helped to increase the accuracy of supervised classification, namely, using LULC indices in addition to original bands of satellite image, increased both kappa and total accuracy. Likewise, using 40 trees in Random Forest algorithm instead 10 trees, for example, helped to achieve higher accuracy in all our classified images.

During the study period, a fast land use change occurred in the study area. Majority of area during 1985 was covered by bare soil and croplands that were without vegetation during the summer, in contrast, in 2021 most of the study area was occupied by built-up class. Also, vegetated areas declined during the study period. These fast land use changes reflect of change in character of the land in terms of absorbing and reflecting the heat during the day and night, increasing impervious materials in the new urbanised area that lead to returned water to underground and increasing possibility of flush flood during raining huge amount of precipitation during winter.

Our results have shown that bare soil area recorded higher surface temperature than all other three main classes (built-up, vegetation and water). Replacing bare soils with built-up areas means decreasing surface temperature during summer daytime. In contrast, replacing vegetated areas with built-up materials leads to an increased surface temperature in Baghdad. In addition, vegetation and moisture indices showed a strong inverse relationship with surface temperature meaning that increasing vegetation such as parks in the city and moisture and water bodies could be a promised strategy for policymakers to decrease the temperature of Baghdad.

We recommend the future direction of research consider the relationship between LST and LULC of Bagdad and similar urban areas using day and night data and inter-seasonal images. In our study we used a list of potential LULC factors mainly using satellite images that advantaged in covering spatial area, however, uncertainty in the used data may be considered a limitation of the research. In addition, in the study, we selected three years to represent a period of the study in case of availability and using every year satellite data may display a more comprehensive trend of change.

5. Conclusions

Urban sprawl changes the character of land materials and the temperature of cities such as Bagdad. Landsat images from 1985 to 2021, in addition to sixteen potential factors, were used to assess land use change and its influence on surface temperature of the city. Our findings suggest that during the study period, vegetated places declined by 39% while built-up areas increased by 139%. During daytime of summer, bare soil experienced the highest surface temperature. In addition, analyzed vegetation and moisture indices have a strong negative relationship with surface temperature, therefore increasing vegetation and water bodies leads to decrease temperature. Applying these strategies helps policymakers to address new problems rising from urban sprawl during the period of global warming around the world.

Funding: The research received no funds.

Data availability: Data can be provided upon request from the corresponding author.

Conflict of interest: The author declares no conflict of interest.

References

Abdul-Hammed, A.N., Mahdi, A.S., 2022. Monitoring Vegetation Area in Baghdad Using Normalized Difference Vegetation Index. Iraqi Journal of Science 1394–1401. https://doi.org/10.24996/ijs.2022.63.3.40

Ali, A.K.M., Ramahi, F.K.M.A., 2020. A study of the Effect of Urbanization on Annual Evaporation Rates in Baghdad City Using Remote Sensing. Iraqi Journal of Science 2142–2149. https://doi.org/10.24996/ijs.2020.61.8.29

Amiri, R., Weng, Q., Alimohammadi, A., Alavipanah, S.K., 2009. Spatial-temporal dynamics of land surface temperature in relation to fractional vegetation cover and land use/cover in the Tabriz urban area, Iran. Remote sensing of environment 113, 2606–2617.

Azad Rasul, Heiko Balzter, Claire Smith, 2016. Diurnal and Seasonal Variation of Surface Urban Cool and Heat Islands in the Semi-Arid City of Erbil, Iraq. Climate. https://doi.org/10.3390/cli4030042

Cai, G., Du, M., 2009. Relationship between thermal inertia and urban heat sink in Beijing derived from satellite images, in: 2009 Joint Urban Remote Sensing Event. IEEE, pp. 1–5.

Carlson, T.N., Arthur, S.T., 2000. The impact of land use—land cover changes due to urbanization on surface microclimate and hydrology: a satellite perspective. Global and planetary change 25, 49–65.

Ermida, S.L., Soares, P., Mantas, V., Göttsche, F.-M., Trigo, I.F., 2020. Google earth engine open-source code for land surface temperature estimation from the landsat series. Remote Sensing 12, 1471.

Frey, C.M., Rigo, G., Parlow, E., Marçal, A., 2005. The cooling effect of cities in a hot and dry environment, in: Global Developments in Environmental Earth Observation from Space, Proceedings of the 25th Annual Symposium of the European Association of Remote Sensing Laboratories, Porto, Portugal. pp. 6–11.

Goldblatt, R., Rivera Ballesteros, A., Burney, J., 2017. High spatial resolution visual band imagery outperforms medium resolution spectral imagery for ecosystem assessment in the semi-arid brazilian sertão. Remote Sensing 9, 1336.

Goldblatt, R., You, W., Hanson, G., Khandelwal, A., 2016. Detecting the boundaries of urban areas in india: A dataset for pixel-based image classification in google earth engine. Remote Sensing 8, 634.

Haubrock, S.-N., Chabrillat, S., Lemmnitz, C., Kaufmann, H., 2008. Surface soil moisture quantification models from reflectance data under field conditions. International journal of remote sensing 29, 3–29.

Iraq Population (2022) - Worldometer [WWW Document], 2022. URL https://www.worldometers.info/world-population/iraq-population/ (accessed 7.3.22).

Jiang, Z., Huete, A.R., Didan, K., Miura, T., 2008. Development of a two-band enhanced vegetation index without a blue band. Remote Sensing of Environment 112, 3833–3845. https://doi.org/10.1016/j.rse.2008.06.006

Kalnay, E., Kanamitsu, M., Kistler, R., Collins, W., Deaven, D., Gandin, L., Iredell, M., Saha, S., White, G., Woollen, J., 1996. The NCEP/NCAR 40-year reanalysis project. Bulletin of the American meteorological Society 77, 437–472.

Li, S., Mo, H., Dai, Y., 2011. Spatio-temporal pattern of urban cool island intensity and its eco-environmental response in Chang-Zhu-Tan urban agglomeration. Communications in Information Science and Management Engineering 1.

Liou, Y.-A., Le, M.S., Chien, H., 2018. Normalized difference latent heat index for remote sensing of land surface energy fluxes. IEEE Transactions on Geoscience and Remote Sensing 57, 1423–1433.

McFeeters, S.K., 1996. The use of the Normalized Difference Water Index (NDWI) in the delineation of open water features. International journal of remote sensing 17, 1425–1432.

Owen, T.W., Carlson, T.N., Gillies, R.R., 1998. An assessment of satellite remotely-sensed land cover parameters in quantitatively describing the climatic effect of urbanization. International journal of remote sensing 19, 1663–1681.

Rasul, A., Balzter, H., Ibrahim, G.R.F., Hameed, H.M., Wheeler, J., Adamu, B., Ibrahim, S., Najmaddin, P.M., 2018. Applying Built-Up and Bare-Soil Indices from Landsat 8 to Cities in Dry Climates. Land 7, 81. https://doi.org/10.3390/land7030081

Rasul, A., Balzter, H., Smith, C., 2015. Spatial variation of the daytime Surface Urban Cool Island during the dry season in Erbil, Iraqi Kurdistan, from Landsat 8. Urban Climate, Cooling Heat Islands 14, 176–186. https://doi.org/10.1016/j.uclim.2015.09.001

Rasul, A., Balzter, H., Smith, C., Remedios, J., Adamu, B., Sobrino, J.A., Srivanit, M., Weng, Q., 2017. A Review on Remote Sensing of Urban Heat and Cool Islands. Land 6, 38. https://doi.org/10.3390/land6020038

Rasul, A., Hameed, H.M., Ibrahim, G.R.F., 2021. Dramatically increase of built-up area in Iraq during the last four decades. Advanced Remote Sensing 1, 1–9.

Rouse, J.W., Hass, R.H., Schell, J.A., Deering, D.W., 1973. Monitoring vegetation systems in the great plains with ERTS. Third Earth Resources Technology Satellite (ERTS) Symposium, 1, 309-317.

sentinel-hub, 2019. EVI (Enhanced Vegetation Index) [WWW Document]. URL https://www.sentinel-hub.com/eoproducts/evi-enhanced-vegetation-index-0 (accessed 5.7.20).

sentinel-hub, 2018. NDVI (Normalized Difference Vegetation Index) [WWW Document]. sentinel-hub.com. URL https://www.sentinel-hub.com/eoproducts/ndvi-normalized-difference-vegetation-index (accessed 5.7.20).

Shigeta, Y., Ohashi, Y., Tsukamoto, O., 2009. Urban Cool Island in daytime-analysis by using thermal image and air temperature measurements, in: The Seventh International Conference on Urban Climate.

Traore, M., Lee, M.S., Rasul, A., Balew, A., 2021. Assessment of land use/land cover changes and their impacts on land surface temperature in Bangui (the capital of Central African Republic). Environmental Challenges 4, 100114.

 doi:10.20944/preprints202207.0248.v1

Watson, C., 2012. Analysis of urban heat island climates along the I-85/I-40 corridor in central North Carolina. The University of North Carolina at Greensboro.

Wilson, E.H., Sader, S.A., 2002. Detection of forest harvest type using multiple dates of Landsat TM imagery. Remote Sensing of Environment 80, 385–396.

Xian, G., Shi, H., Zhou, Q., Auch, R., Gallo, K., Wu, Z., Kolian, M., 2022. Monitoring and characterizing multi-decadal variations of urban thermal condition using time-series thermal remote sensing and dynamic land cover data. Remote Sensing of Environment 269, 112803.